ADVANCED OPTICAL MATERIALS

PHOTODETECTORS

J. A. Rogers and co-workers exploit a design for visible-blind ultraviolet detection using silicon photodiodes and down-shifting luminophores. The fabricated device exhibits a selective UV response between 300 nm and 360 nm, which exceeds that in the visible range by about 103. An array of such detectors demonstrates the potential for using these structures in UV imagers, and suggests compatibility with large-area, CMOS-compatible Si electronics and photonics.

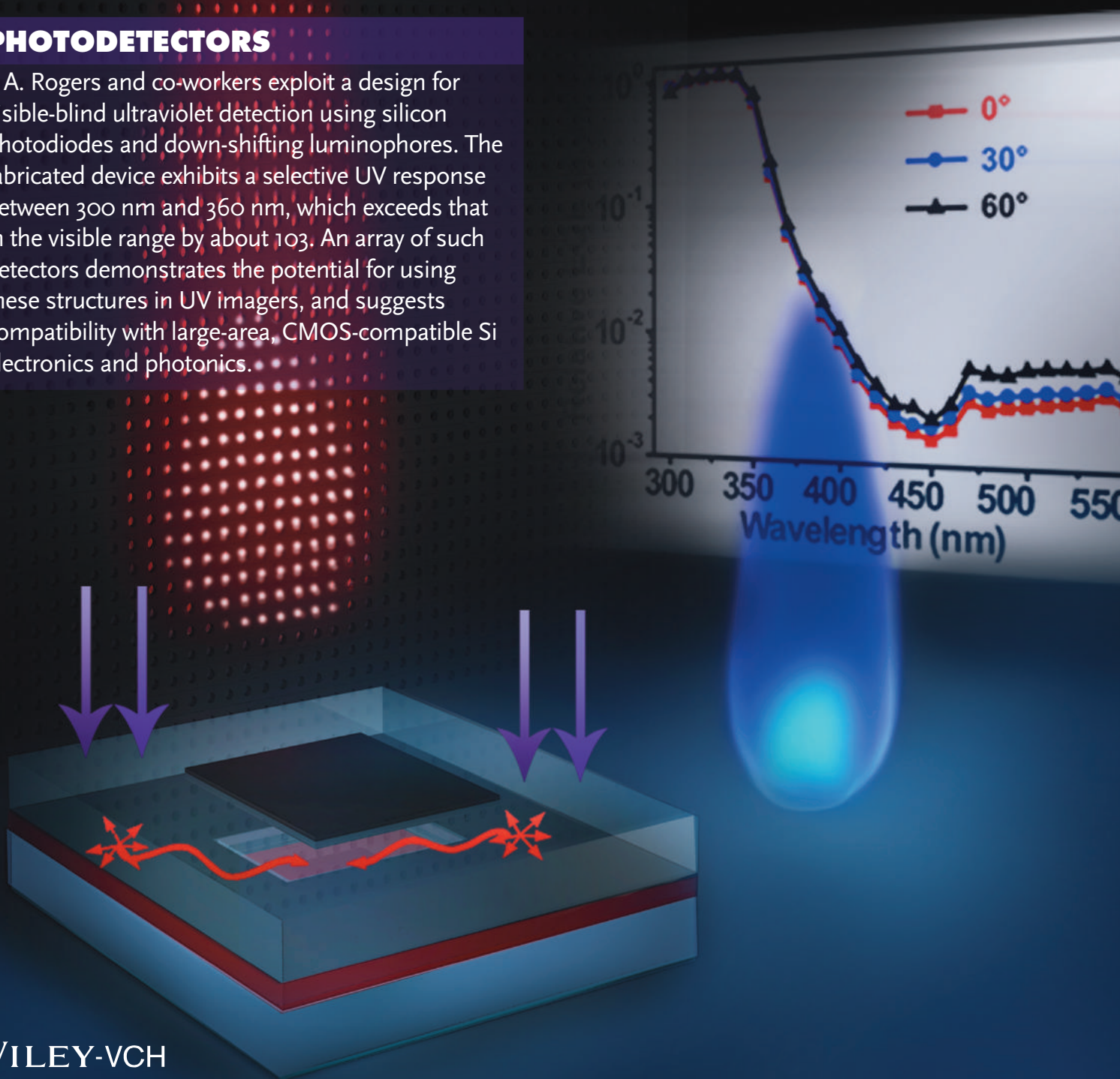

WILEY-VCH

Silicon-Based Visible-Blind Ultraviolet Detection and Imaging Using Down-Shifting Luminophores

*Xing Sheng, Cunjiang Yu, Viktor Malyarchuk, Yu-Heng Lee, Seungho Kim, Taehwan Kim, Ling Shen, Chris Horng, Jordan Lutz, Noel C. Giebink, Jongwook Park, and John A. Rogers**

Photon detection and imaging devices for selective use in the ultraviolet (UV) spectral range are of interest for use in applications that include flame detection, chemical sensing, astronomical observation, communications and health care.[1–10] Of particular value are visible-blind and solar-blind UV detectors, with selective responses at wavelengths below 400 nm and 280 nm respectively.[1–3] In these detectors, low sensitivities for visible and infrared (IR) light ensure robust measurement capabilities in the UV with minimal background. Traditional UV detectors based on photomultiplier tubes[4] are attractive but require require bulky, vacuum based components. Recent work shows the ability to form visible-blind and solar-blind UV detectors using large bandgap semiconductors like AlGaN,[5] diamond,[6] ZnO[7,8] and certain organic materials[9] to provide attractive alternatives. A common disadvantage, however, is that these materials, by comparison to silicon, are difficult to grow/deposit in high purity, uniform layers, to dope in controlled ways and/or to process at large areas with low costs. Devices that combine UV bandpass filters with silicon detectors avoid these limitations, but they suffer from intrinsically low responses in the UV (effective quantum efficiency < 30%), limited lifetimes due to degradation under prolonged UV exposure and difficulties in fabricating the necessary filters.[10–14] Some such filters use alkali metals,[11,13] which require advanced packaging structures to prevent oxidation, while others exploit sub-wavelength photonic crystals,[14] whose fabrication can be difficult. Here we present a self-powered, visible-blind UV detection design that exploits Si based photodetectors with UV down-shifting luminophores in structures for light trapping and management. Specifically, a europium (Eu) complex dispersed poly(methyl methacrylate) (PMMA) film coated on top of a Si detector serves as a luminescent waveguide to enable selective UV responses from 300 nm to 360 nm. The obtained ratio of photoresponses in the UV (300–360 nm) and the visible (>400 nm) is ~10^2–10^3. Demonstration experiments illustrate the ability of such devices to detect UV emitted from invisible methanol flames. A simple imaging system that incorporates 256 multiplexed detectors illustrates the scalability of the ideas.

Dr. X. Sheng, Dr. V. Malyarchuk, C. Horng, J. Lutz, Prof. J. A. Rogers
Department of Materials Science and Engineering and Frederick Seitz Materials Research Laboratory
University of Illinois at Urbana-Champaign
Urbana, IL, 61801, USA
E-mail: jrogers@illinois.edu

Prof. C. Yu
Department of Mechanical Engineering
University of Houston
Houston, TX, 77204, USA

Y.-H. Lee
Department of Electronic Materials Engineering
The Australian National University
Canberra, ACT 0200, Australia

S. Kim, Prof. J. Park
Department of Chemistry
The Catholic University of Korea
Yokkok, Bucheon, Kyunggi, 420–743, Korea

T. Kim, Prof. N. C. Giebink
Department of Electrical Engineering
The Pennsylvania State University
University Park, PA, 16802, USA

Dr. L. Shen
Department of Physics, College of Sciences
China University of Mining and Technology
Xuzhou, Jiangsu, 221116, PR China

DOI: 10.1002/adom.201300475

The europium (Eu^{3+}) complex (structure shown as an inset in **Figure 1**a), Eu(DPEPO)(hfac)$_3$ [DPEPO = bis(2-(diphenylphosphino)phenyl)ether oxide, hfac = hexafluoroacetylacetonate] or EuDH, serves as the UV down-shifting material.[15] The absorption and emission spectra for the EuDH dissolved in methylene dichloride (CH_2Cl_2) appear in Figure 1a. The EuDH absorbs photons with wavelengths from 250 nm to 360 nm and emits at ~610 nm. Thermogravimetric analysis (TG) and differential scanning calorimetric (DSC) results in Figure 1b indicate that the EuDH has a melting temperature at 164 °C and exhibits mass loss above 340 °C due to chemical decomposition. EuDH powder can be mixed into a solution of PMMA in anisole to yield a dispersion that can be spin cast on various substrates. Figure 1c presents the absorption spectra of such films (40 μm thick) with different EuDH concentrations on quartz substrates. While the pure PMMA film is transparent above 300 nm, the EuDH doped PMMA films with concentrations larger than 5 wt% strongly absorb between 300 nm and 360 nm and emit red light. The photoluminescence quantum yield (PLQY) (measured by an excitation at 337 nm) is 0.77 ± 0.04, and the PL decay lifetime is (0.75 ± 0.05) ms (Figure 1d). Figure 1e presents photographs of a quartz substrate coated with EuDH-doped PMMA under ambient light and UV illumination. Release from the quartz yields flexible films, capable of lamination onto other target surfaces (Figure 1f).

Figure 2a schematically illustrates the design of a visible-blind UV detector formed by combining a EuDH-doped

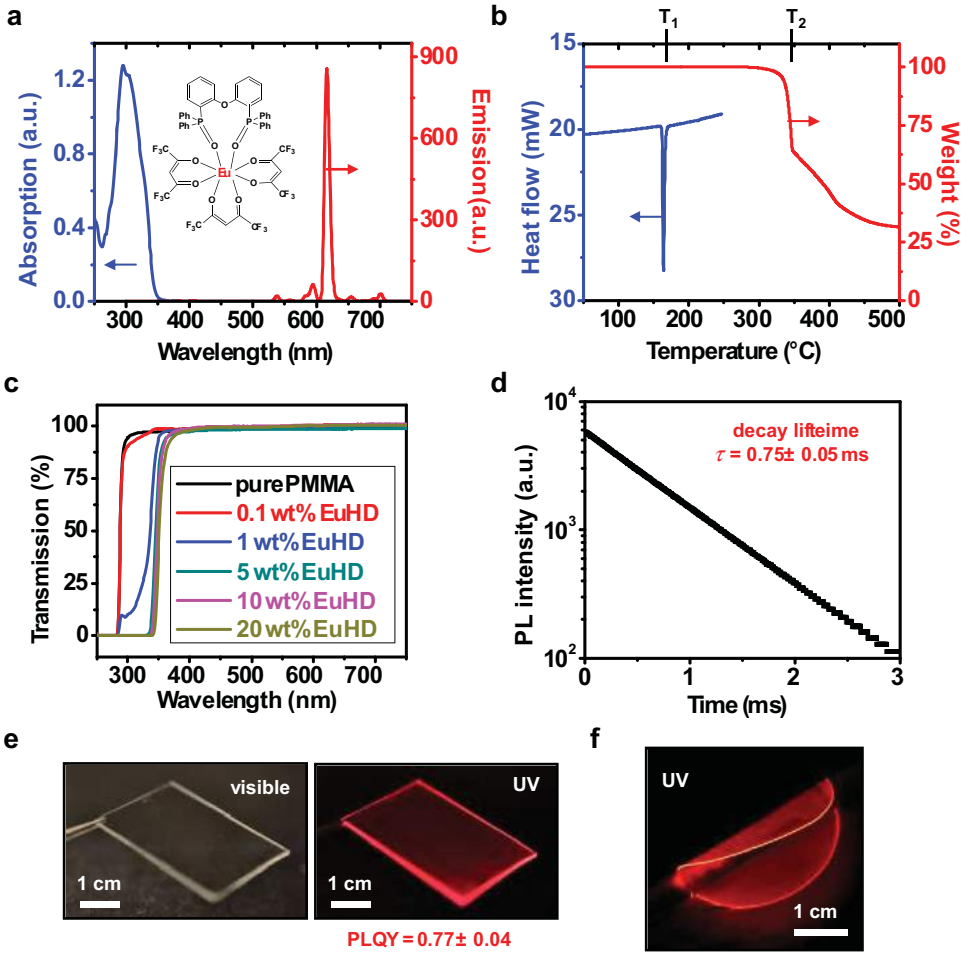

Figure 1. a) Absorption and emission spectra of EuDH in CH_2Cl_2. Inset: molecular structure of EuDH. b) Thermal analysis (TG and DSC) of EuDH, showing a melting temperature T_1 = 164 °C and a decomposition temperature T_2 = 340 °C. c) Transmission spectra of 40 μm EuDH doped PMMA films coated on quartz, with different concentrations. d) Photoluminescence decay for EuDH doped in PMMA, showing a PL decay lifetime of (0.75 ± 0.05) ms. e) Photographs of a quartz substrate coated with EuDH doped PMMA (10 wt%, 40 μm) under ambient visible light and UV illuminations, with a PLQY of 0.77 ± 0.04. f) UV Photograph of a flexible, freestanding EuDH doped PMMA film.

PMMA film and a Si photodiode. The overall device area under illumination is 1 cm × 1 cm. The photodiode uses a pn junction design with active area of 500 μm × 500 μm, fabricated on a 300 μm thick Si wafer, using conventional diffusion doping and lithographic process.[16,17] After metallization and encapsulation with a polyimide film (3 μm), a thin coating of Au (100 nm thick) serves as a specular reflector on regions of the silicon substrate adjacent to the photodiode. A similar Au film lies on top of an overcoat of EuDH-doped PMMA (10 wt%; 40 μm thick), located directly above the photodiode and with a slightly larger size (700 μm × 700 μm). Specular reflection by these two Au films ensures that incoming light with wavelengths outside of the spectral region of absorption by the EuDH does not reach the photodiode. A fraction of the luminescent light that follows from absorption in the EuDH-doped PMMA layer (300–360 nm) transports laterally by waveguiding until it is absorbed and detected by the Si photodiode. This architecture not only blocks photons outside of the UV range, but also converts the UV photons to a wavelength (~610 nm) that is favorable for detection with Si and concentrates this light by processes of lateral waveguiding. Calculated efficiency of optical coupling into the Si photodiode is calculated by ray tracing and plotted in Figure S7 as a function of the size of the illuminion area. The coupling efficiency in the current design (~1%) is mostly limited by the isotropic photon re-emission.

Figure 2b shows the measured external quantum efficiency (EQE) spectra for different device configurations (Figure S3) at normal incidence with monochromatic illumination at wavelengths between 300 nm to 550 nm. The EQE results are normalized so that the highest EQE achieved in the design with both EuDH and top Au layer (red curve, at 330 nm) is unity (100%). As expected, the isolated Si detector exhibits low and high EQE in the UV and visible ranges, respectively. UV absorption in the 3 μm polyimide encapsulating layer (Figure S4) along with high recombination losses near the top surface of the Si detector, contribute to the poor UV response. Addition of a film of EuDH-doped PMMA improves the UV responses significantly due to down-shifting and waveguiding concentration.[18–20] The

Adv. Optical Mater. 2014,
DOI: 10.1002/adom.201300475

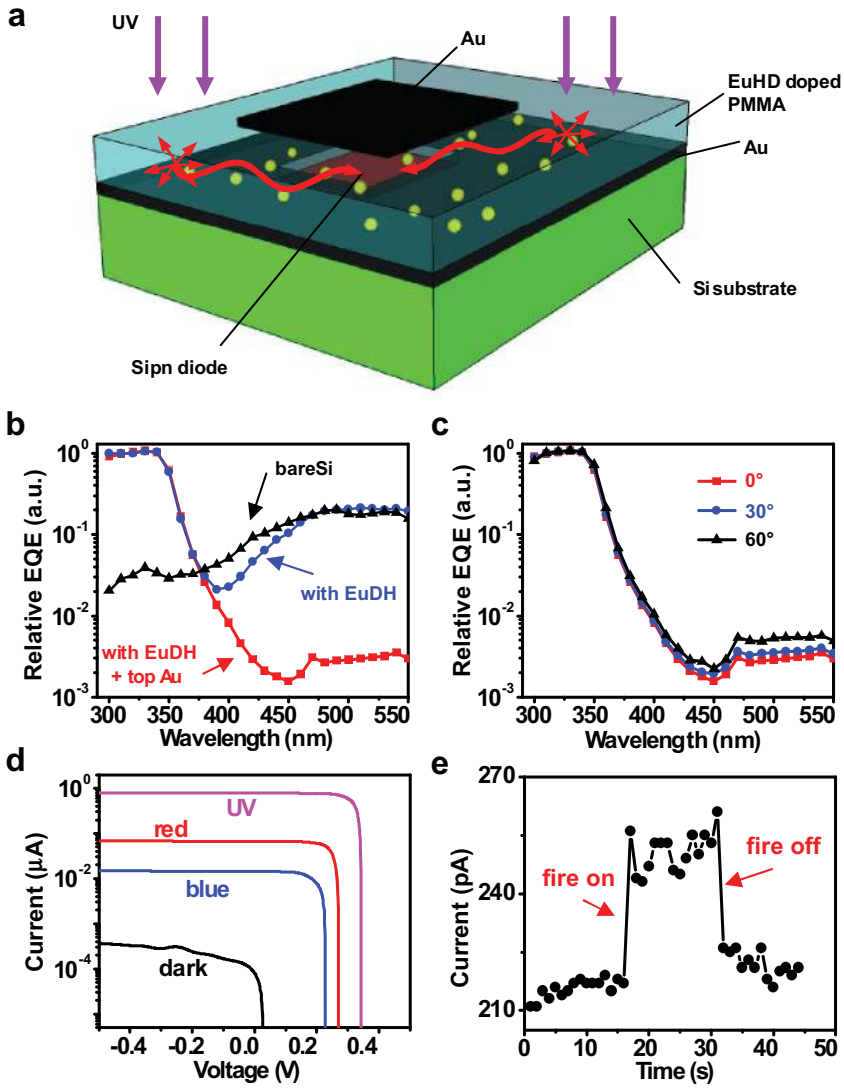

Figure 2. a) Schematic illustration of the visible blind UV detector design. b) EQE spectra of different device configurations shown in Figure S3 at normal incidence. c) EQE spectra of the device shown in Figure 2a at different incident angles. d) Current-voltage characteristics under dark, UV (365 nm), blue (470 nm) and red (625 nm) illuminations, with intensity of 5 mW/cm^2. e) Photocurrent measured with methanol fire on and off under ambient light illumination.

visible responses, however, remain high because visible light can pass directly into the detector. The top metal layer blocks this direct illumination. For the device shown in Figure 2a, the UV responses reach their peak values between 300 nm and 360 nm and then decrease significantly at wavelengths longer than 360 nm, consistent with the absorption spectra measured for EuDH-doped PMMA films in Figure 1c. The highest ratios between responses in the UV and the visible are 10^3:1, obtained by comparing the EQE values at 340 nm and 450 nm. Illumination at oblique angles (30° and 60°, shown in Figure 2c) increases the visible response ($\lambda > 400$ nm), but the ratios remain greater than 10^2:1. Non-zero EQE values in the visible arise mainly from scattered and non-collimated light that reaches the Si diode.

Figure 2d presents current–voltage characteristics measured during normal incidence illumination at an intensity of 5 mW/cm^2 for wavelengths of 365 nm, 470 nm, and 625 nm. Consistent with the EQE results of Figure 2b, the photocurrent under UV illumination is much larger than that obtained under blue and red illumination. It should be noted that the photocurrents reported here are captured under zero bias voltage, thereby demonstrating the ability to operate without external power sources. An example application involves the use of this self-powered UV detector to detect methanol flames, which are invisible in ambient light due to selective emission in the UV and IR regions (see Supporting Movie taken with a commercial CCD camera). The UV emission can be efficiently measured by our detector even in ambient light, with minimal noise from the background (Figure 2e).

Figure 3 explores capabilities in spatial resolution for UV imaging applications. Here, scanning a detector across an alternating pattern of white and black lines (period, *P*) illuminated by a collimated UV LED (365 nm) yields spatial variations in

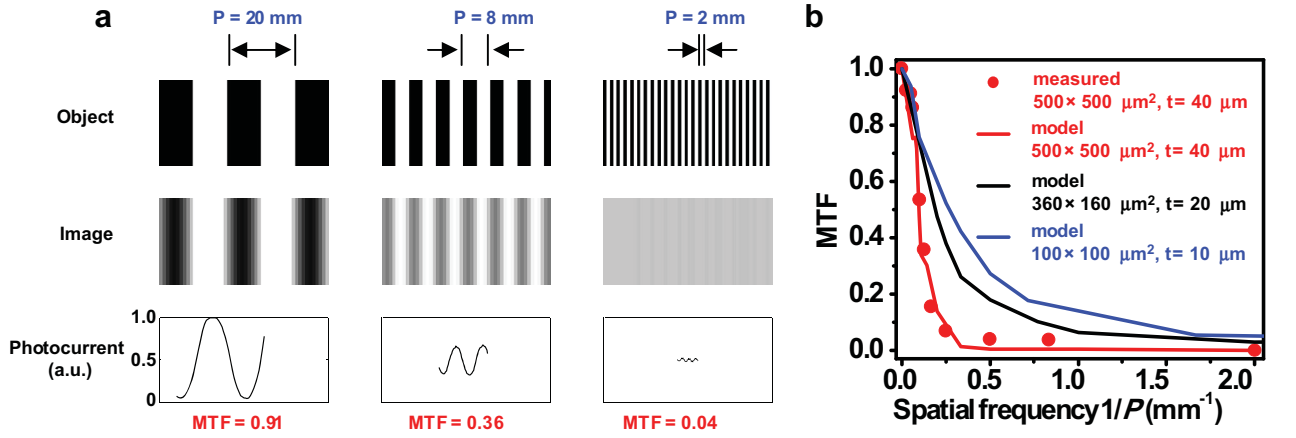

Figure 3. a) Captured 1D images by scanning the detector across patterns with different periods. Photocurrents are recorded as a function of scanning distances. b) Experimentally obtained MTF, in comparison with simulation results based on different device dimensions.

photocurrent. The resolution performance can be characterized by a modulation transfer function (MTF),

$$MTF = \frac{I_{max} - I_{min}}{I_{max} + I_{min}} \quad (1)$$

where I_{max} and I_{min} are the maximum and minimum photocurrents, respectively. The MTF values as a function of spatial frequency ($1/P$) appear in Figure 3b, together with calculations based on ray tracing simulation. This model, which uses the device configuration shown in Figure 2a (detector size 500 μm × 500 μm, PMMA thickness 40 μm), yields results that agree with the measured MTF. The resolution is mainly defined by the effects of waveguiding in the luminescent PMMA layer. Additional modeling results suggest that further improvement of the MTF can be achieved by reducing the Si diode size and the PMMA layer thickness, as shown in Figure 3b, because reduced diode size leads to a smaller cross-section in capturing photons emitted far away from the diode, and thinner PMMA layer increases the optical loss for photons propagating at a longer distance. Smaller diode size and thinner PMMA layer are also beneficial for flexible/stretchable device array operation because of the smaller flexural rigidity and ability to accommodate larger strain.[21,22]

Figure 4a shows a picture of a multiplexed array of UV photodetectors, collected under illumination with UV light. Blocking diodes co-integrated with the photodetectors provide a means for multiplexed addressing. The p-n-p diode array, which includes blocking diodes for multiplexed readout, is fabricated on a silicon-on-insulator (SOI) wafer (1.5 μm thick top silicon thickness), interconnected and transferred onto a glass substrate using previously described methods.[16,17] Here, sizes of the photodiodes are 360 μm × 160 μm, and the thickness of EuDH-doped PMMA layer is 20 μm. The spacing between adjacent pixels is 1 mm. Figure 4d presents an equivalent circuit for a unit cell and Figure 4e shows the current–voltage responses from a single p-n-p photodiode in the dark and with UV illumination. The yield is ~94% (240 working photodiodes out of 256). Tests of imaging capabilities involve passing collimated UV light (365 nm) through transparency masks. An automated data acquisition and processing system[17] enables image capture, as illustrated for the case of line art (letters 'UI' and 'C') in Figure 4e. The current image quality is limited by the optical and electrical crosstalk in the Si diode array, as well as the photocurrent sensitivity of the image acquisition system. An imaging system with higher performance could potentially be achieved by using commercial Si CCD arrays with optimal device geometries (detector size, spacing, luminescent layer thickness, etc.). For example, shrinking the current array design by a factor of 10 (reaching a detector spacing of 0.1 mm and a PMMA thickness of 1 μm) will enable a denser array design, potentially achieving 300 × 300 pixels in a 3 cm × 3 cm Si chip, which provides a low-cost, more easily-scalable route to imaging systems compared to devices based on non-Si techniques.

In summary, this paper introduces a strategy for visible-blind UV photodetection and imaging, by combined use of down-shifting luminescent materials and light trapping structures with conventional Si photodetectors. Such concepts appear readily adaptable to large-area Si based image sensors made by CMOS compatible processes, thereby providing a low-cost route to high resolution UV imaging. With appropriate luminophores,[23] band-selective photdetection in different UV spectral ranges can be achieved. UV responses for such a design can be further improved, for example, by optimizing the Si photodiodes, choosing luminophores with PLQY > 100% via multi-exciton generation,[24] and creating photonic structures with controlled anisotropic emissions.[25] To obtain an image sensing array with higher resolution performance, smaller pixels and thinner luminescent layers can be employed. Tradeoffs between device resolution and sensitivity must, of course, be addressed for practical applications. In addition, each pixel can be isolated by using reflective sidewalls to improve coupling efficiency and eliminate the optical crosstalk, which is associated with the luminescent scattering and limits the optical resolution of our current device (Figure 3). Alternatively, more advanced image processing algorithms can be employed to reconstruct high quality images.[26] The integrated image array can also be released from the rigid substrate and formed on a curvilinear surface (Figure S6), enabling unusual optoelectronic systems for various applications.[16,17] The design concept presented

Adv. Optical Mater. 2014,
DOI: 10.1002/adom.201300475

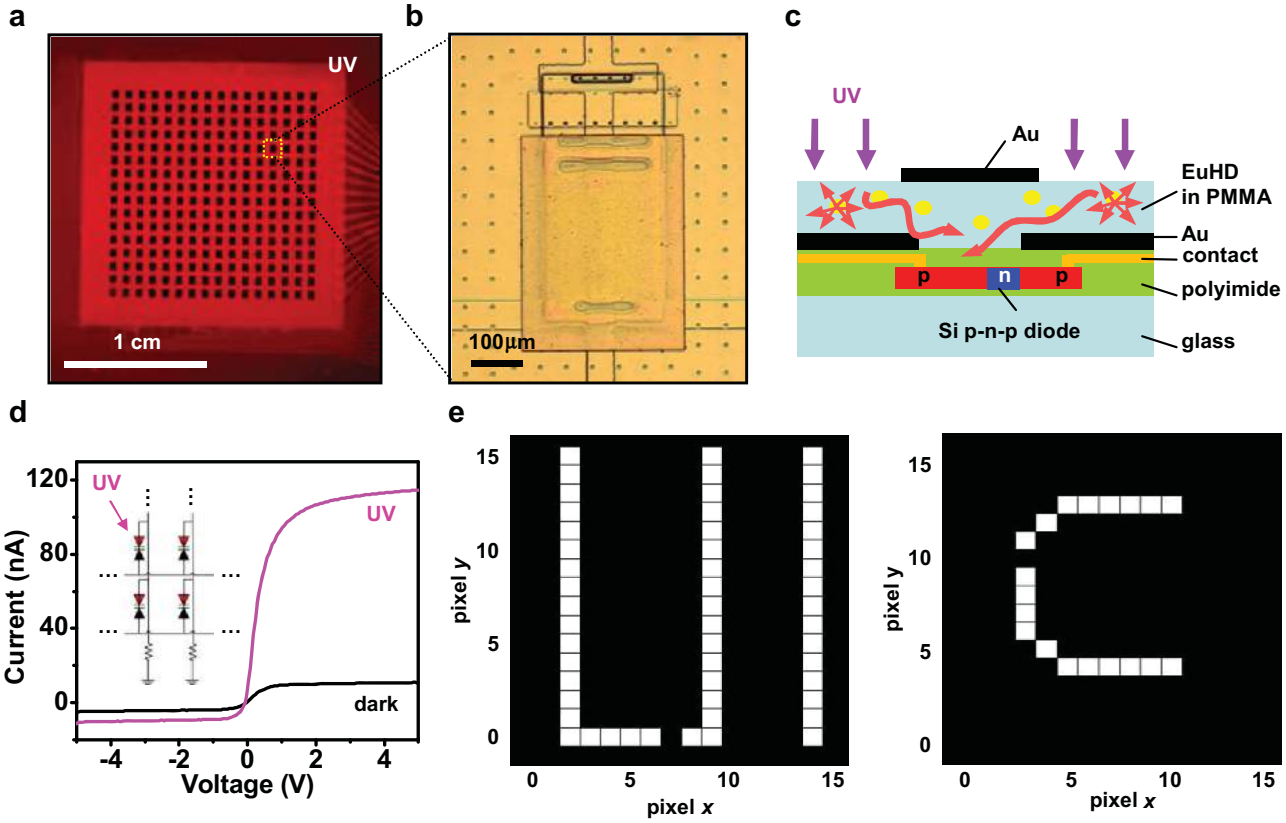

Figure 4. a) UV photograph of a 16 × 16 UV detector array. b) Microscopic image of a single pixel, made by a p-n-p Si diode. c) Schematic cross-sectional view of the detector design. d) Current–voltage characteristics of a single pixel. Inset: circuit diagram. e) Representative image results for letters 'UI' and 'C'.

here provides a feasible and low-cost way for UV detection systems in selective bands.

Experimental Section

EuDH Preparation and Characterization: The EuDH compound is synthesized by mixing europium (hexafluoroacetylacetonate)$_3$ (Rare Earth Products, Inc.) and bis(2-(diphenylphosphino)phenyl)ether oxide (Strem Chemicals, Inc.) in a solution of 1:1 H_2O:Ethanol at 60 °C, followed by purification and recrystallization.[15,27] The resulting EuDH compound (purity > 95%) can be characterized by NMR spectroscopy (Figure S1). EuDH is mixed with a PMMA solution (950PMMA A11, 11 wt% in anisole, MicroChem Corp.), spin cast and cured at 150 °C for an hour, to form films with different thicknesses and concentrations. The formed PMMA film has a refractive index of about 1.5 at 600 nm.

Optical Measurements: EuDH powders are dissolved into methylene dichloride (CH_2Cl_2) (concentration 5×10^{-5} mol/L) for optical absorption and emission tests (excitation wavelength at 320 nm). The transmission spectra of EuDH-doped PMMA films are collected using a UV-vis spectrometer (Cary 5G, Varian, Inc.). The PLQY and PL decay measurements are performed at an excitation wavelength of 337 nm, using an integrating sphere and a Si photodetector. A mercury-vapor lamp (Blak-Ray, UVP, LLC) is used to provide UV illumination for photographs.

Device Fabrication: Si-based photodetectors are fabricated on Si wafers (Figure 2a) and SOI wafers (Figure 4a) as previously reported (also see Figure S2 and Figure S5).[16,17] Doping in selected areas is conducted by solid-state diffusion. Detector arrays formed on SOI wafers are isolated and transferred onto glass substrates for subsequent process. Lithographically defined Cr/Au metals (10 nm/300 nm) by sputtering are used for interconnects, and polyimide films (3 μm) are spin coated as interlayer dielectrics and encapsulants. The substrates are then covered with 100 nm Au by electron beam evaporation, with only the active photodiode area exposed. The active device sizes are 500 μm × 500 μm and 360 μm × 160 μm, for devices shown in Figure 2a and Figure 4a, respectively. EuDH doped PMMA layers are spin coated and baked to form the down-shifting layer. Finally, another 100 nm Au layer (700 μm × 700 μm in Figure 2a and 500 μm × 300 μm in Figure 4a) is deposited on top of the PMMA by E-beam evaporation to cover the active diode area.

Device Characterization: Monochromatic light from 300 nm to 550 nm is generated and chopped using a Xenon arc lamp (Acton Research Corp.) coupled to a monochrometer (Jarrell-Ash Monospec 18), with intensity calibrated by a standard GaP detector (Thorlabs, Inc.). Photocurrent is collected by a lock-in amplifier (SR830, Stanford Research Sys., Inc.). The current-voltage relation is measured by a source meter (Keithley 2400) under illumination by collimated LEDs with different colors (UV 365 nm, blue 470 nm, red 625 nm, all from Thorlabs, Inc.). The illumination area is 1 cm × 1 cm.

Imaging Acquisition: A collimated UV LED (365 nm) is used as a light source, passing through patterns printed on transparency masks. Imaging scanning in Figure 3a is performed by attaching the detector to a controlled translation stage. Ray tracing simulations are performed by Matlab codes.[19] Imaging acquisition is conducted using a data multiplex circuit and automated processing algorithms.[17]

Supporting Information

Supporting Information is available from the Wiley Online Library or from the author.

Acknowledgements

X. Sheng and C. Yu contributed equally to this work. This work is supported by the DOE 'Light-Material Interactions in Energy Conversion' Energy Frontier Research Center under grant DE-SC0001293. C. Yu acknowledges the start-up funding support from the Department of Mechanical Engineering, the Cullen College of Engineering, and the Division of Research at the University of Houston. S. Kim and J. Park are supported by the National Research Foundation of Korea (NRF) grant funded by the Korea government (MEST) (No. 2012001846). T. Kim and N. Giebink acknowledge support from the DOE SunShot concentrating solar power program under award number DE-EE0005798. L. Shen acknowledges support from China Scholarship Council.

Received: November 15, 2013
Revised: December 23, 2013
Published online:

[1] M. Razeghi, A. Rogalski, *J. Appl. Phys.* **1996**, *79*, 7433.
[2] M. Razeghi, *Proc. IEEE* **2002**, *90*, 1006.
[3] E. Monroy, F. Omnes, F. Calle, *Semicond. Sci. Technol.* **2003**, *18*, R33.
[4] R. W. Engstrom, Photomultiplier Handbook RCA Corp., New Jersey, USA **1980**.
[5] E. Cicek, R. McClintock, Z. Vashaei, Y. Zhang, S. Gautier, C. Y. Cho, M. Razeghi, *Appl. Phys. Lett.* **2013**, *102*, 051102.
[6] A. Balducci, M. Marinelli, E. Milani, M. E. Morgada, A. Tucciarone, G. Verona-Rinati, M. Angelone, M. Pillon, *Appl. Phys. Lett.* **2005**, *86*, 193509.
[7] Y. Liu, C. R. Gorla, S. Liang, N. Emanetoglu, Y. Lu, H. Shen, M. Wraback, *J. Electron. Mater.* **2000**, *29*, 69.
[8] W. Yang, S. S. Hullavarad, B. Nagaraj, I. Takeuchi, R. P. Sharma, T. Venkatesan, R. D. Vispute, H. Shen, *Appl. Phys. Lett.* **2003**, *82*, 3424.
[9] D. Ray, K. L. Narasimhan, *Appl. Phys. Lett.* **2007**, *91*, 093516.
[10] R. S. Popovic, K. Solt, U. Falk, Z. Stoessel, *Sensor. Actuat. A-Phys.* **1990**, *A21–A23*, 553.
[11] R. W. Wood, *Phys. Rev.* **1933**, *44*, 353.
[12] M. M. Blouke, M. W. Cowens, J. E. Hall, J. A. Westphal, A. B. Christensen, *Appl. Opt.* **1980**, *19*, 3318.
[13] J. T. Clarke, W. R. Skinner, M. B. Vincent, T. Irgang, V. Suratkal, H. Grassl, J. T. Trauger, *Appl. Opt.* **1999**, *38*, 1803.
[14] W. Li, S. Y. Chou, *Opt. Express* **2010**, *18*, 931.
[15] O. Moudam, B. C. Rowan, M. Alamiry, P. Richardson, B. S. Richards, A. C. Jones, N. Robertson, *Chem. Commun.* **2009**, 6649.
[16] H. C. Ko, M. P. Stoykovich, J. Song, V. Malyarchuk, W. M. Choi, C. Yu, J. B. Geddes III, J. Xiao, S. Wang, Y. Huang, J. A. Rogers, *Nature* **2008**, *454*, 748.
[17] Y. M. Song, Y. Xie, V. Malyarchuk, J. Xiao, I. Jung, K. Choi, Z. Liu, H. Park, C. Lu, R. Kim, R. Li, K. B. Crozier, Y. Huang, J. A. Rogers, *Nature* **2013**, *497*, 95.
[18] J. Yoon, L. Li, A. V. Semichaevsky, J. H. Ryu, H. T. Johnson, R. G. Nuzzo, J. A. Rogers, *Nat. Comm.* **2011**, *2*, 343.
[19] X. Sheng, L. Shen, T. Kim, L. Li, X. Wang, R. Dowdy, P. Froeter, K. Shigeta, X. Li, R. G. Nuzzo, N. C. Giebink, J. A. Rogers, *Adv. Energy Mater.* **2013**, *3*, 991.
[20] X. Sheng, C. J. Corcoran, J. He, L. Shen, S. Kim, J. Park, R. G. Nuzzo, J. A. Rogers, *Phys. Chem. Chem. Phys.* **2013**, *15*, 20434.
[21] D. H. Kim, J. Xiao, J. Song, Y. Huang, J. A. Rogers, *Adv. Mater.* **2010**, *22*, 2108.
[22] J. A. Rogers, M. G. Lagally, R. G. Nuzzo, *Nature* **2011**, *477*, 45.
[23] W. M. Yen, S. Shionoya, H. Yamamoto, Phosphor Handbook Taylor & Francis Group, LLC, Florida, USA **2006**.
[24] V. Sukhovatkin, S. Hinds, L. Brzozowski, E. H. Sargent, *Science* **2009**, *324*, 1542.
[25] N. C. Giebink, G. P. Wiederrecht, M. R. Wasielewski, *Nat. Photonics* **2011**, *5*, 694.
[26] A. Koppelhuber, O. Bimber, *Opt. Express* **2013**, *21*, 4796.
[27] H. Xu, L. Wang, X. Zhu, K. Yin, G. Zhong, X. Hou, W. Huang, *J. Phys. Chem. B* **2006**, *110*, 3023.